Supplement of Geosci. Model Dev., 15, 4393–4424, 2022
https://doi.org/10.5194/gmd-15-4393-2022-supplement

Geoscientific Model Development
Open Access
EGU

Supplement of

Ocean biogeochemistry in the Canadian Earth System Model version 5.0.3: CanESM5 and CanESM5-CanOE

James R. Christian et al.

Correspondence to: James R. Christian (jim.christian@ec.gc.ca)

Supplementary Table S1 - List of CMIP6 experiments conducted with CanESM5-CanOE. The list of experiments conducted with CanESM5 is much more extensive and is not detailed here. Note that all realizations are numbered r*i1p2f1, i.e., the p1 model was retired before any CanESM5-CanOE experiments were run.

MIP	Experiment	# of realizations
CMIP	piControl	500 y
CMIP	historical	3
CMIP	esm-piControl	500 y
CMIP	esm-hist	3
CMIP	1pctCO2	1
ScenarioMIP	ssp126	3
ScenarioMIP	ssp245	3
ScenarioMIP	ssp370	3
ScenarioMIP	ssp585	3
C4MIP	1pctCO2-bgc	1
C4MIP	1pctCO2-rad	1
C4MIP	esm-ssp585	3
CDRMIP	esm-pi-cdr-pulse	3
CDRMIP	esm-pi-CO2-pulse	3
OMIP	omip1	1

Supplementary Table S2 - Alkalinity sources and sinks associated with nitrogen cycle processes in moles of alkalinity equivalent per mole of N. Positive value indicates alkalinity source.

Process	Alkalinity source/sink
Phytoplankton NH_4 uptake	-1
Phytoplankton NO_3 uptake	+1
Organic N remineralization	+1
N_2 fixation	+1
Nitrification (NH_4 oxidation to NO_3)	-2
Denitrification	+1
Annamox	0

Supplementary Table S3 - Other CMIP6 models used in the cross-model analyses. Model (source ID), centre, and variable names are official CMIP6 names. CanESM5 and CanESM5-CanOE data are r1i1p2f1.

Source ID	Centre	Country	Variables used	Variant
ACCESS-ESM1-5	CSIRO	Australia	dfe	r1i1p1f1
CESM2	NCAR	US	dfe, dissic, no3, so, thetao, talk	r1i1p1f1
CESM2-WACCM	NCAR	US	dissic, so, thetao, talk	r1i1p1f1
CNRM-ESM2-1	CNRM-CERFACS	France	dfe, dissic, epc100, no3, o2, so, thetao, talk	r1i1p1f2
GFDL-CM4	NOAA-GFDL	US	dfe, dissic, o2, so, thetao, talk	r1i1p1f1
GFDL-ESM4	NOAA-GFDL	US	dfe, dissic, epc100, no3, o2, so, thetao, talk	r1i1p1f1
IPSL-CM6A-LR	IPSL	France	dissic, o2, so, thetao, talk	r32i1p1f1
MIROC-ES2L	MIROC	Japan	dfe, dissic, o2, so, thetao, talk	r1i1p1f2
MPI-ESM-1-2-HAM	HAMMOZ-Consortium	Germany	dfe, no3, o2, so, thetao	r1i1p1f1
MPI-ESM1-2-LR	MPI-M	Germany	dfe, dissic, epc100, no3, o2, so, thetao	r1i1p1f1
MPI-ESM1-2-HR	MPI-M	Germany	dissic, no3, o2, so, thetao, talk	r1i1p1f1
MRI-ESM2-0	MRI	Japan	dissic, o2, so, thetao	r1i2p1f1
NorESM2-LM	NCC	Norway	dfe, dissic, epc100, no3, o2	r1i1p1f1
NorESM2-MM	NCC	Norway	dissic, no3, o2, so, thetao	r1i1p1f1
UKESM1-0-LL	MOHC	UK	dfe, dissic, epc100, no3, o2, so, thetao, talk	r1i1p1f2

Supplementary Table S4 - Correlation of CanESM5 and observed DIC on six depth horizons for five different ensemble members.

Depth	r1i1p2f1	r2i1p2f1	r3i1p2f1	r4i1p2f1	r5i1p2f1
100	0.722	0.724	0.713	0.714	0.722
400	0.828	0.827	0.822	0.824	0.830
900	0.815	0.811	0.808	0.811	0.815
1300	0.873	0.872	0.871	0.873	0.874
1750	0.887	0.886	0.886	0.887	0.888
3500	0.868	0.866	0.866	0.865	0.866

Supplementary Table S5 - Latitude and longitude boundaries used for spatial averaging of regions (Figures 10, 14, 16, 17). In Figure 10, Western Subarctic Pacific and Eastern Subarctic Pacific are combined as “North Pacific” (latitude boundaries as below). A map of the regions is shown in Figure S5.

Region	S bound	N bound	W bound	E bound
North Atlantic	45N	65N	50W	10W
Western Subarctic Pacific	40N	52N	160E	160W
Eastern Subarctic Pacific	40N	52N	160W	130W
Southern Ocean		30S		
Tropical Pacific	2S	2N	180	76W
Tropical Atlantic	5S	5N	30W	0

Supplementary Table S6 - Net change in total ocean DIC content (PgC) over 165 years with (Historical experiment) or without (corresponding years of piControl experiment) anthropogenic CO_2 emissions for selected CMIP6 models. piControl values are calculated by linear regression; Historical values are calculated by difference of pentad means (2010-2014 minus 1850-1854).

Source ID	piControl	Historical
CanESM5	-5.1	127.9
CanESM5-CanOE	-10.0	117.7
CESM2	-36.4	123.9
CESM2-WACCM	-54.6	122.5
GFDL-ESM4	7.7	168.6
IPSL-CM6A-LR	31.8	157.9
NorESM2-LM	-24.9	111.0
UKESM1-0-LL	-5.5	130.6

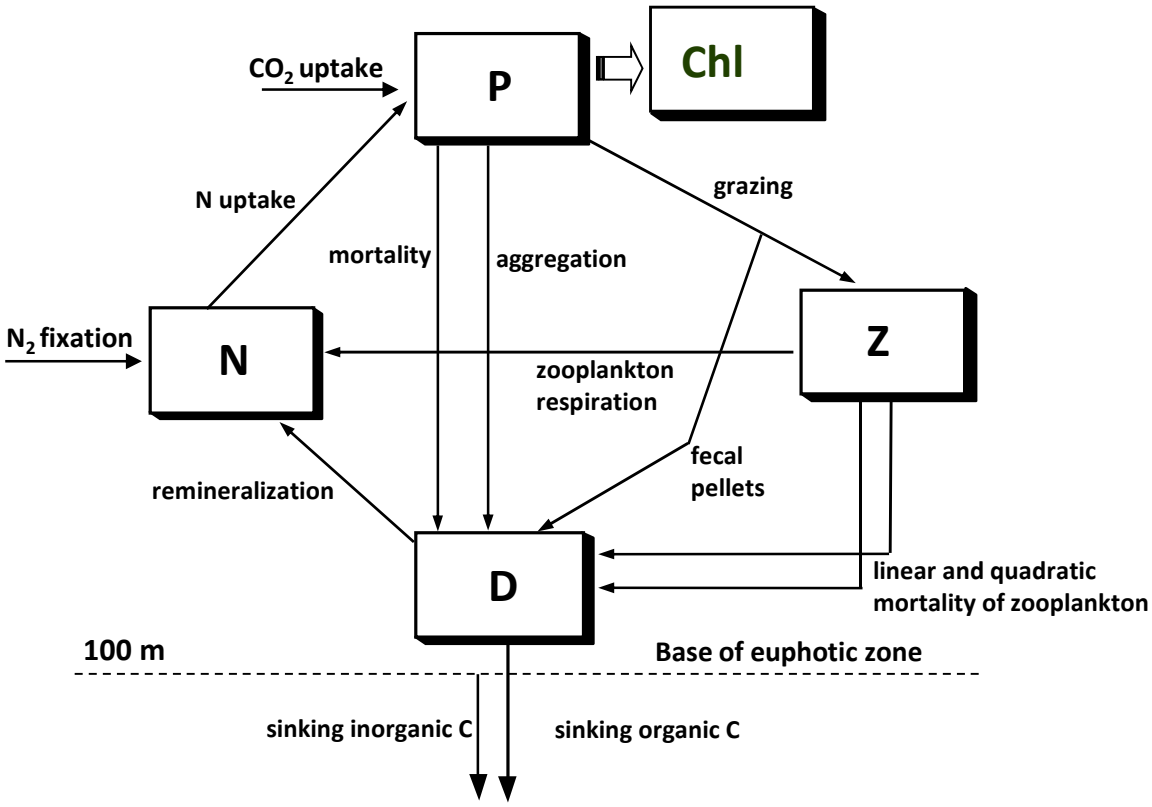

Figure S1 - Schematic of the Canadian Model of Ocean Carbon (CanESM5) food web (after Zahariev et al. (2008) and Christian et al (2010)). All biological compartments (except chlorophyll) are denominated in N units and sources and sinks of DIC are calculated using a fixed Redfield Ratio of 6.625. $CaCO_3$ flux at the base of the euphotic zone is calculated diagnostically (equations 12-14 in Zahariev et al. (2008)).

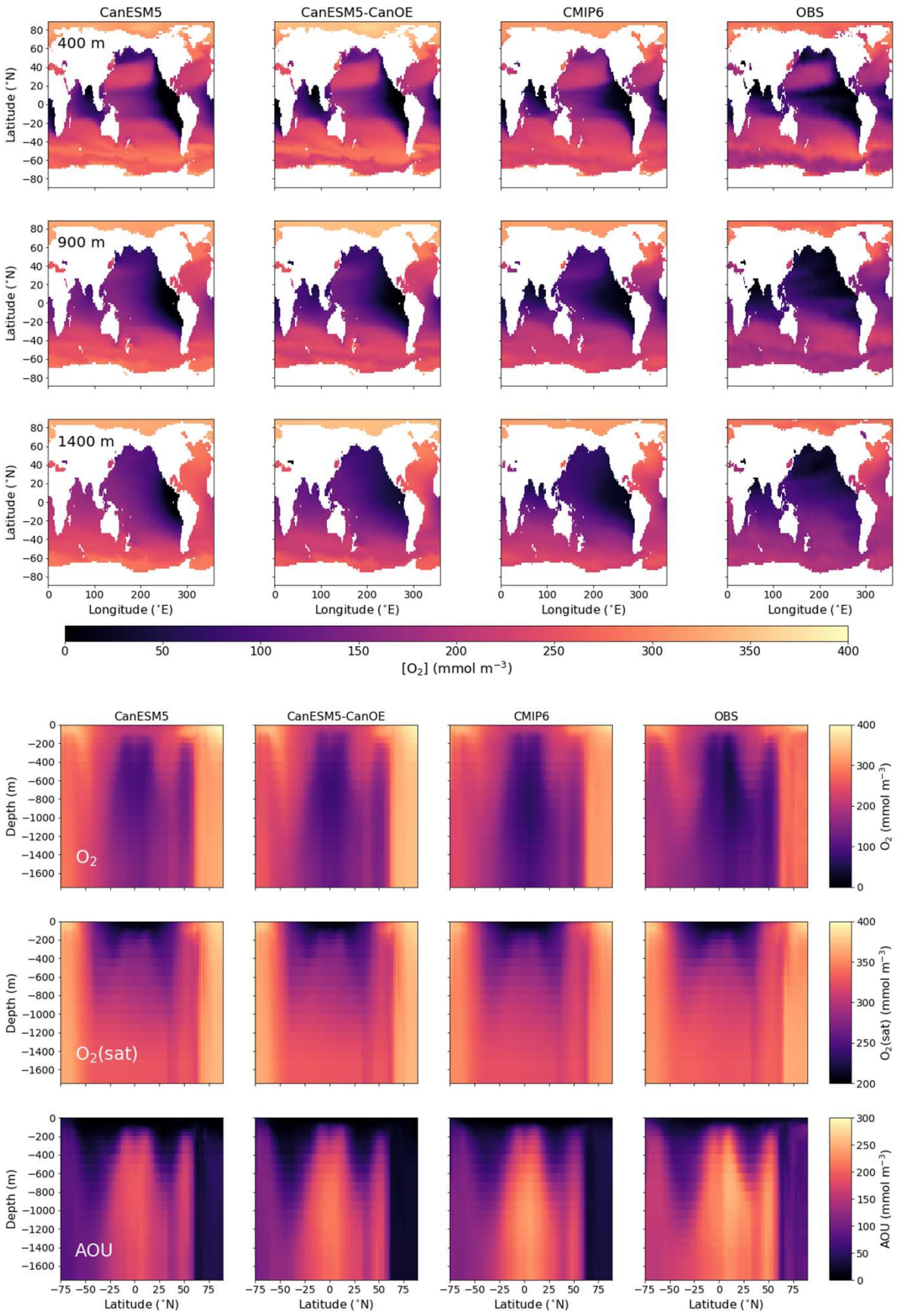

Figure S2 - Alternate versions of Figures 2, 3, 6 and 7 that show model concentrations rather than anomalies. OBS panels are the same as main text figures.

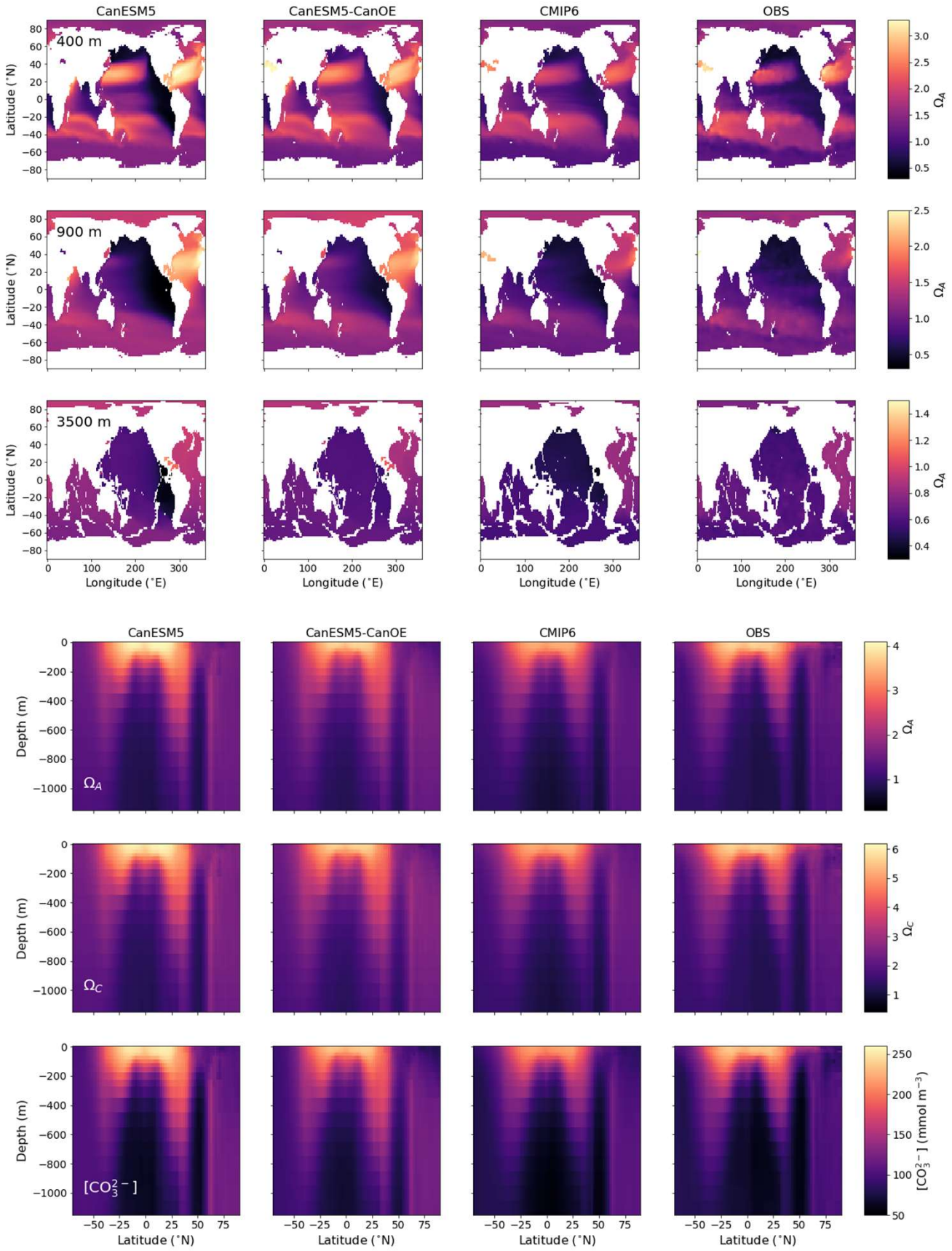

Figure S2 - Alternate versions of Figures 2, 3, 6 and 7 that show model concentrations rather than anomalies. OBS panels are the same as main text figures.

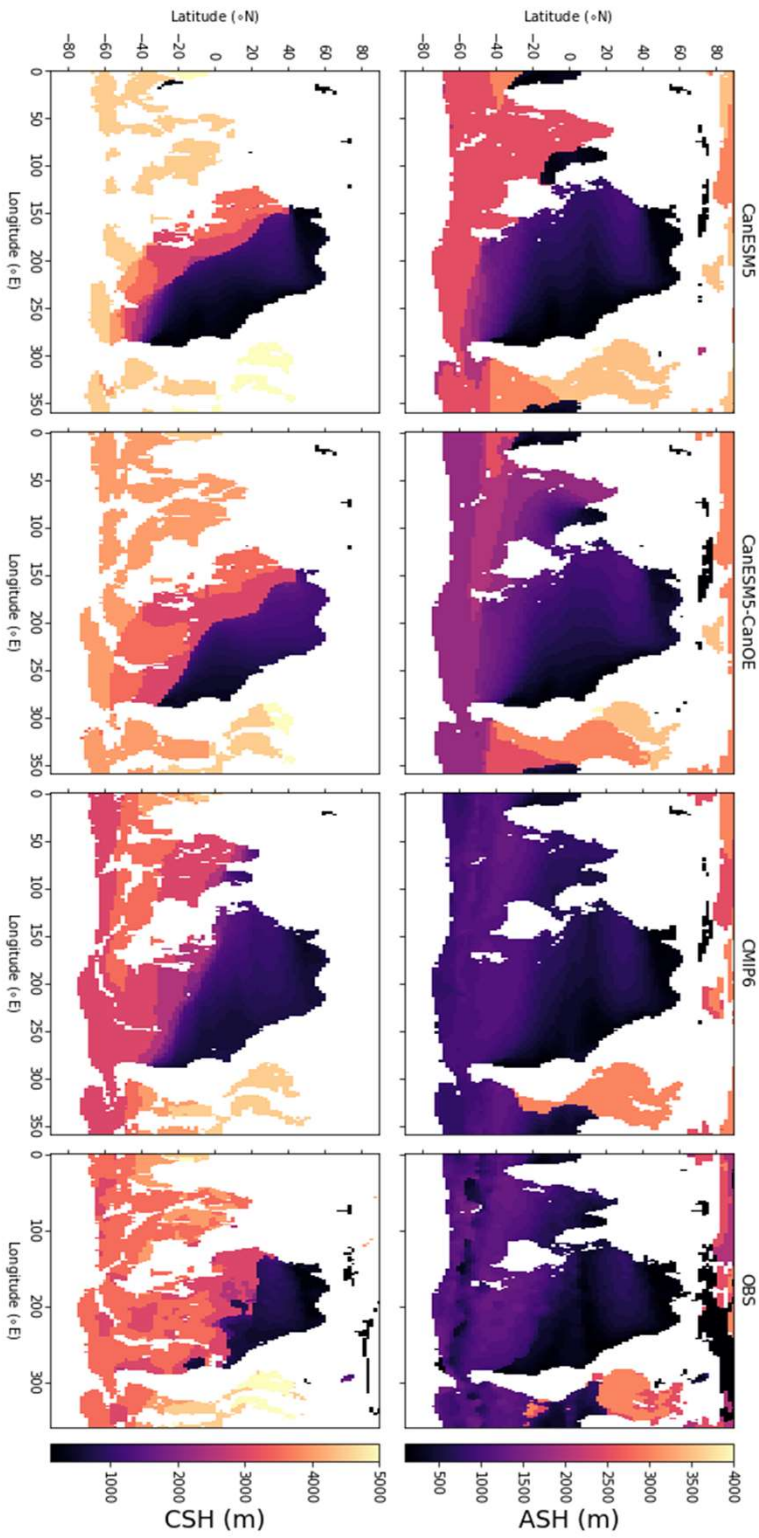

Figure S3 - Depth of the aragonite saturation horizon (ASH) and the calcite saturation horizon (CSH) in CanESM5, CanESM5-CanOE, the model ensemble mean of other CMIP6 models, and an observation based data product (GLODAPv2). Model values calculated from means of 1986-2005 of the historical experiment.

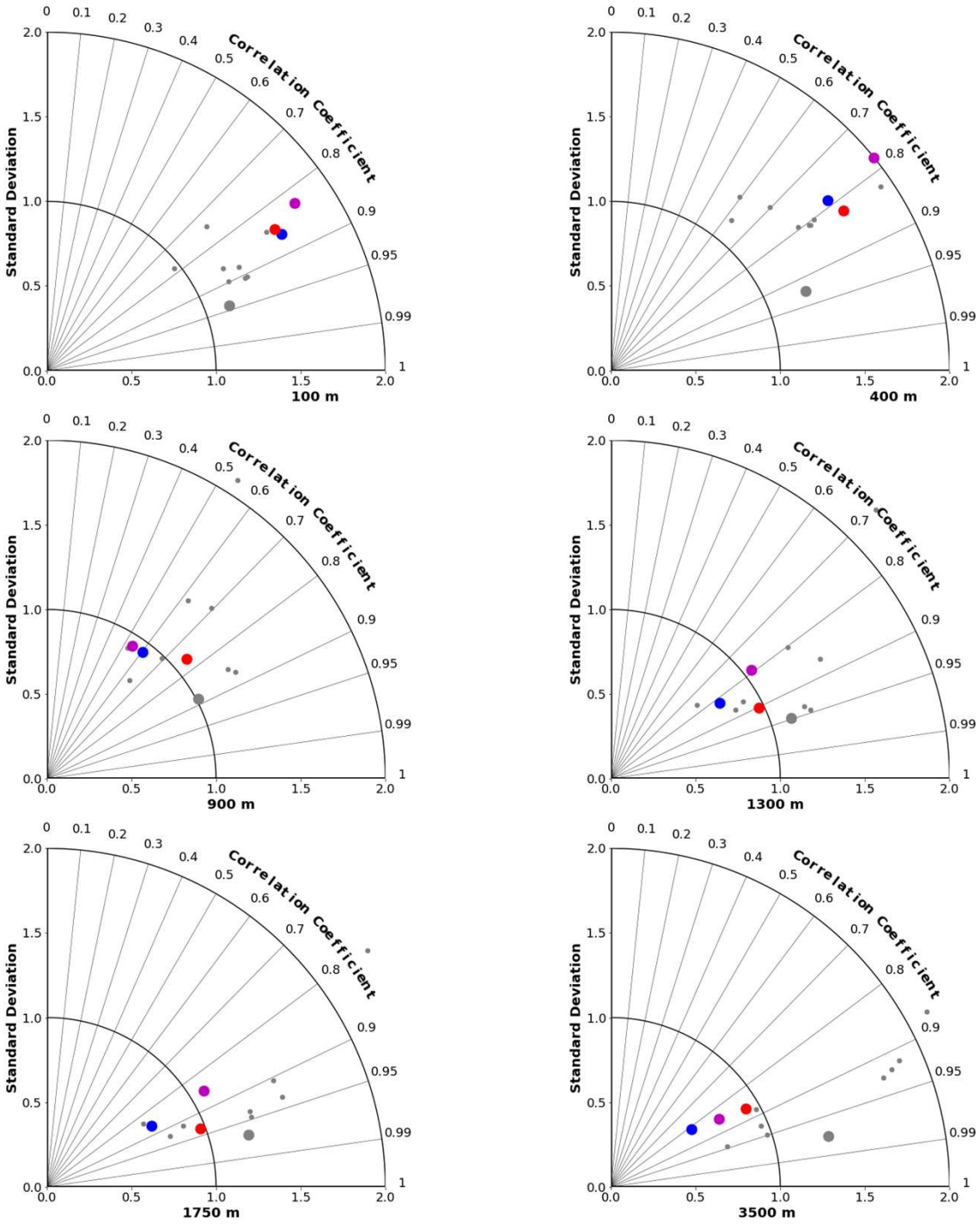

Figure S4 - Taylor diagrams for total alkalinity on various depth horizons. Colour codes and z levels as in Figures 4, 8, and 9.

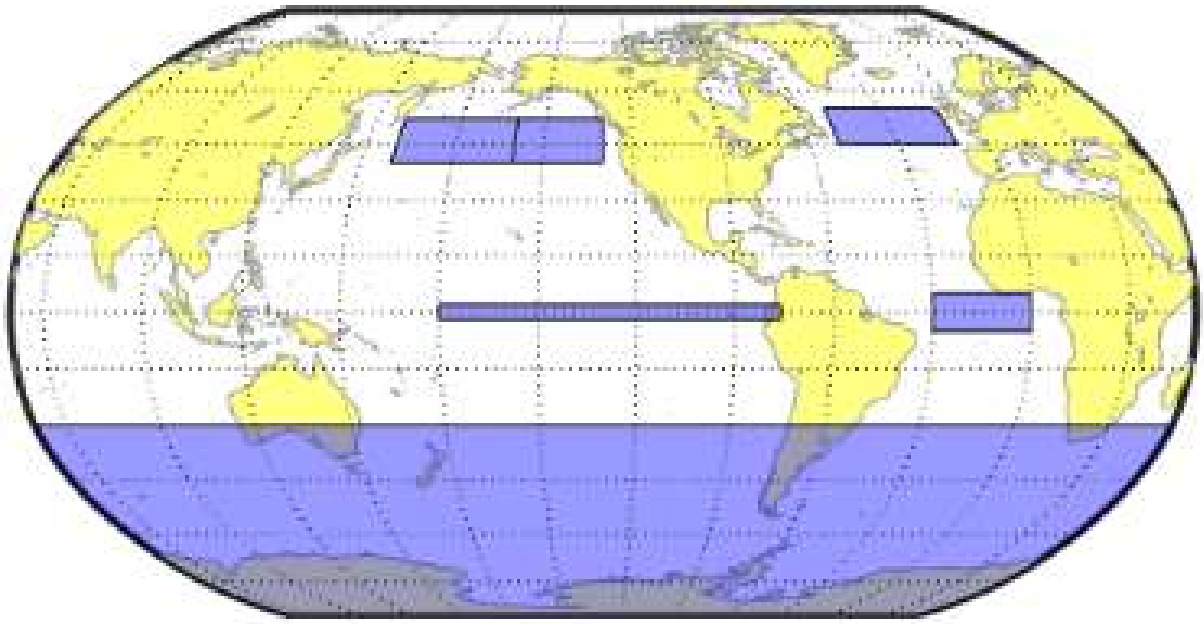

Figure S5 - Map of regions listed in Table S5 (averaging regions used in Figures 10, 14, 16, 17).

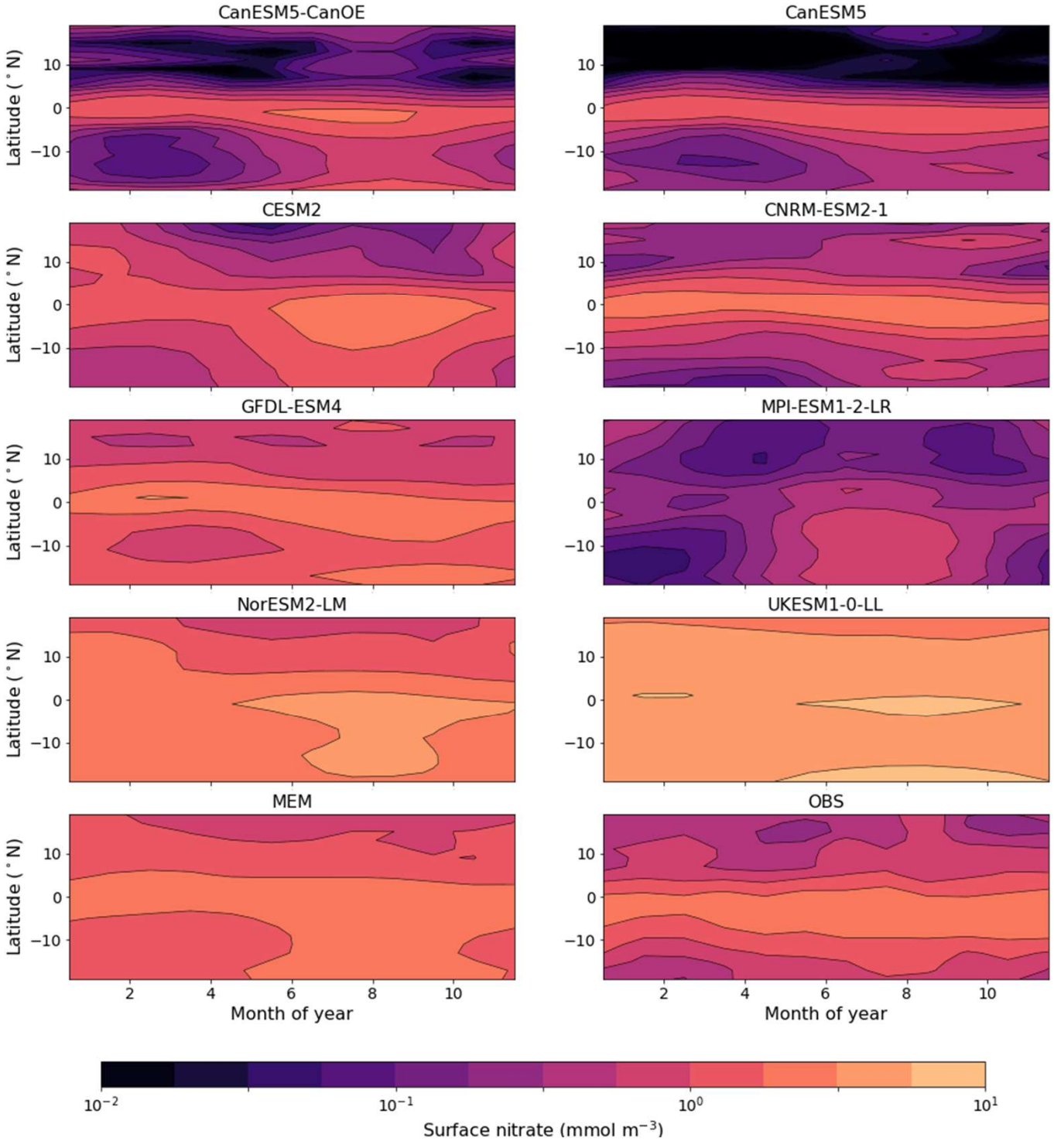

Figure S6 - As Figure 11 but for latitudes <20° only.

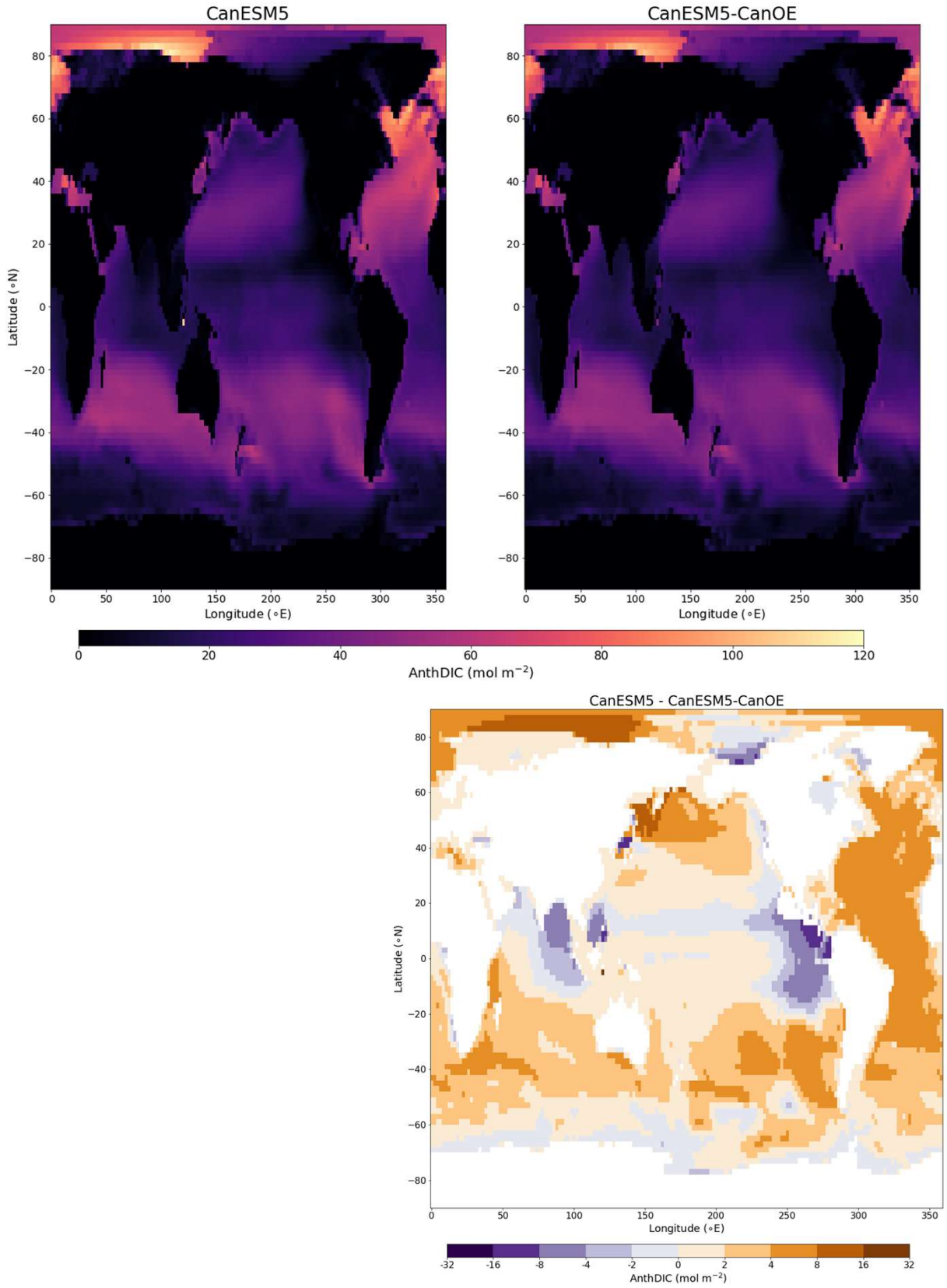

Figure S7 - Column inventory of anthropogenic DIC in CanESM5 and CanESM5-CanOE in molC m^{-2}, calculated as the difference between the mean of the last 10 years of the historical run and the mean of 165 years of piControl. Lower panel is the difference between the two shown on a logarithmic scale.

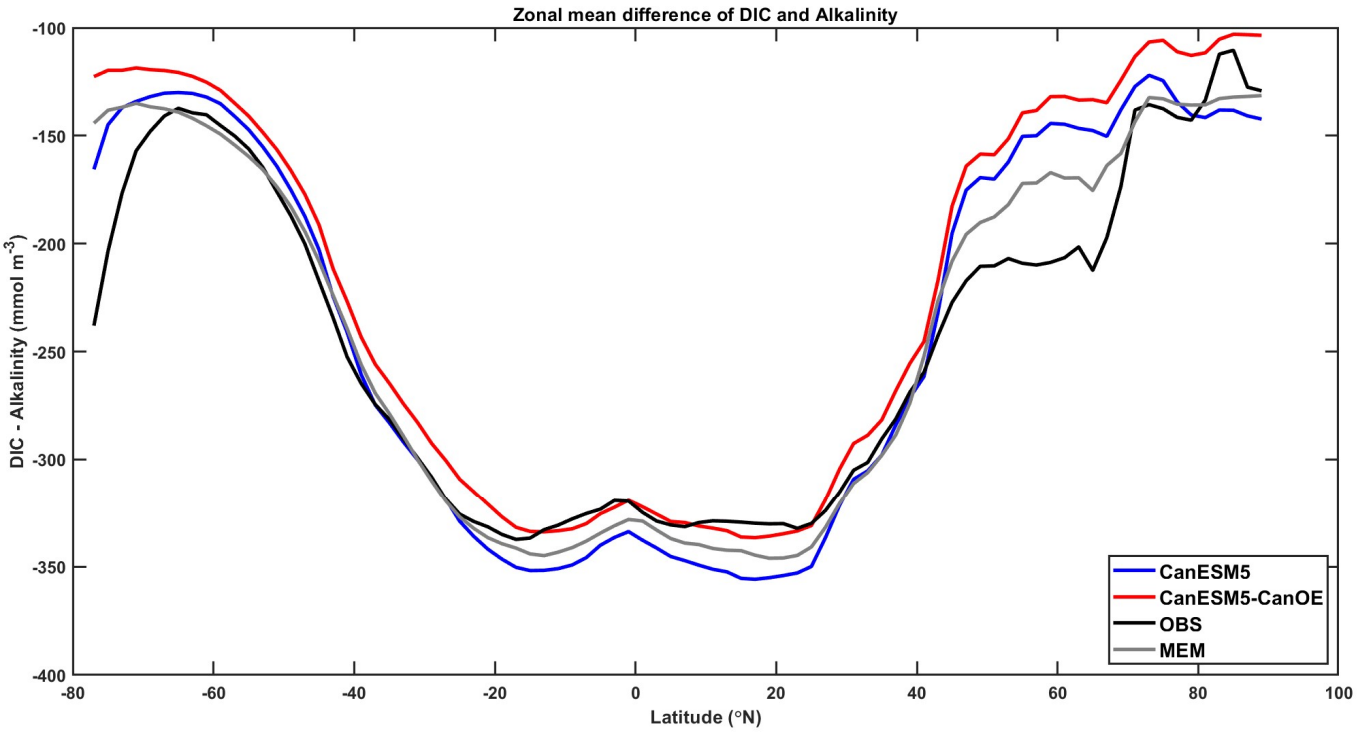

Figure S8 -Difference between zonal mean surface DIC and zonal mean surface alkalinity for CanESM5, CanESM5-CanOE, observations (GLODAPv2), and a model ensemble mean (MEM) of other CMIP6 models (difference of 20 year means for 1986-2005).

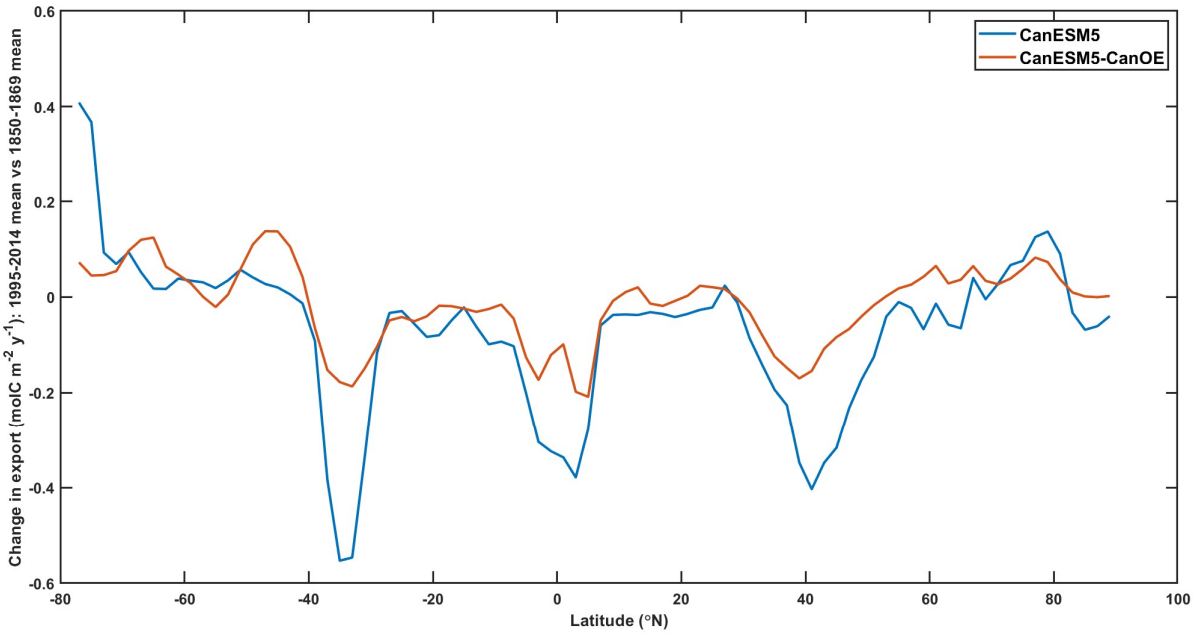

Figure S9 -Change in zonal mean export production in CanESM5 and CanESM5-CanOE over historical experiment (difference of 20 year means for first and last 20 y).

Aeolian iron dissolution

Aeolian iron was introduced assuming a fractional solubility of 1.4% in the surface layer and adopting the PISCES parameterization for subsurface dissolution. According to Aumont et al (2015) this assumes a sinking speed of 2 m/d and a dissolution rate of 0.0001 d^{-1}, which translates to an e-folding length scale of 20000 m and is consistent with the NEMO 3.4 PISCES code, except for the length scale, which is set to a much smaller 1000 m.

We can think of this parameterization as the divergence dF/dz of a flux that declines exponentially with depth:

Fz = F0*exp(-k/w*z)

where k is a first-order dissolution rate and w is the sinking speed (e.g., Christian et al., 1997).

dF/dz = -k/w*Fz

is the input of dissolved iron at depth z.

Because the subsurface layers are much thicker than the surface layer, the total amount of iron introduced results in an effective fractional solubility of aeolian iron that is much larger than the specified 1.4%. The whole water column dissolution is 6.4%, of which 22% is introduced in the surface layer. Note that if the somewhat arbitrary substitution of an e-folding length scale of 1000 m for 20000 m were not done, the difference would be much larger: a net fractional solubility of 25%, of which only 5.5% would go into the surface layer. (All of these numbers are grid-specific and are for the ORCA1 levels.)

Because in our model the rate of scavenging loss is very high for concentrations above 0.6 nM, much of this additional aeolian iron will be removed without ever entering the euphotic zone. While the net dissolution of the total aeolian iron input is much higher than the specified fractional solubility of 1.4%, it is important to note that in terms of biological response it is clearly not equivalent to a model that supplies aeolian Fe only to the surface layer with a fractional solubility of 6.4%. It is probably closer to a model with 1.4% and no subsurface dissolution, although exactly where it falls on this spectrum will vary with region and season.

Aumont, O., C. Ethé, A. Tagliabue, L. Bopp, and M. Gehlen, 2015. PISCES-v2: an ocean biogeochemical model for carbon and ecosystem studies. Geoscientific Model Development 8: 2465–2513.

Christian, J.R., M.R. Lewis, and D.M. Karl, 1997. Vertical fluxes of carbon, nitrogen and phosphorus in the North Pacific Subtropical Gyre near Hawaii. Journal of Geophysical Research 102: 15667-15677.

Dissolved iron model comparison to observations

As there is no gridded global data product for dissolved iron (dFe) we present here some comparisons with individual bottle samples from the GEOTRACES Intermediate Data Product 2017 (Schlitzer et al., 2018), the MBARI data compilation (www3.mbari.org/chemsensor/Data/), and the Pacific data set compiled by PICES WG22 (meetings.pices.int/members/working-groups/disbanded/wg22). The MBARI data include both profile (the "Global Iron Data") and surface transect ("MBARI SOLAS") data (the SOLAS data also include some profiles but are primarily underway surface measurements). The GEOTRACES data are primarily profile data (393 profiles total, only ~10% of 7519 data are <50 m). Most of the MBARI data are also in the PICES data set; these were preprocessed to remove redundant data. Data from the underway surface transects were excluded to avoid overweighting these regions due to autocorrelation, leaving a total of 3575 data points. Concentrations > 2.5 nM, which comprise 1.3% of GEOTRACES data and 3.3% of PICES/MBARI data, were excluded from the model/data comparisons below, except for the individual GA-02 profiles.

Evaluating the CanOE model beyond what has been discussed in the main text identified several key points, most of which have already been made to some degree. CanESM5-CanOE compares favourably with other CMIP6 models but is quite biased towards a 'nutrient-type' rather than 'scavenged-type' profile (Figures S10b, c, e-h). In CanOE rates of Fe scavenging are very high above 0.6 nM dFe and very low below this concentration, resulting in an almost constant deep water concentration of 0.6 nM. The collected data (of which there are >10000 vs only a few hundred in 1997) show that the basic hypothesis articulated by Johnson et al. (1997) still holds: deep-water concentrations are generally close to 0.6 nM, although much higher concentrations are sometimes observed at depths of thousands of metres (Figure S10b, see e.g. Resing et al., 2014). High concentrations are also sometimes observed in near-surface waters (Figure S10b) and CanESM5-CanOE is among the models least able to reproduce these. CanESM5-CanOE consistently overestimates the lowest observed concentrations and underestimates the higher ones (Figure S10d). One might argue that other models do little better in a statistical sense. However, in several models the deviations from the 1:1 line are less systematic than in CanESM5-CanOE; the residuals may be larger but they are more homogeneous. This comparison also largely confirms the results of Séférian et al. (2020, their Figure 5), although only two of the four models shown here were included in their analysis. CNRM-ESM2-1 shows a capacity to simulate the full range of dFe concentrations, as was the case in Séférian et al., although in no case is the spatial pattern correlation very large (in Séférian et al., CNRM-ESM2-1 was the second highest at 0.21). Nonetheless, this analysis indicates that purely statistical comparisons as in Figures S10e-g can be misleading. CanESM5-CanOE shows fairly good skill by these metrics but has systematic biases. These biases can clearly be attributed to the rather simplistic scavenging model employed, and will be addressed in future versions.

We made direct comparisons of our modelled dissolved iron concentrations with GEOTRACES transect data for GA-02 in the Atlantic (e.g., Middag et al. 2015), which was the most spatially extensive transect available (Figure S10a). We show depth profiles from 47°S to 47°N. Mostly this confirms what we already knew from the other analyses presented: our model has a very low scavenging rate below 0.6 nM and a very high rate above, so that deep water concentrations are quite uniform and near-surface concentrations are biased low in high-deposition regions like the northern tropical Atlantic. For the most part, the model reproduces the observed concentrations quite well, given these known biases. What we learn from including this additional analysis is (a) the model is biased high in the Antarctic Bottom Water (Middag et al. 2015 give an excellent presentation of the location and biogeochemical properties of this water mass), and (b) the seasonal biological drawdown in the mid-latitude North Atlantic is weak. The former is probably due mainly to the low scavenging rate at

concentrations <0.6 nM, although it may also indicate a high bias in surface waters of the source region (see section 3.3). The latter is probably related to the generally low rate of export production (Figure 19) and the weak North Atlantic spring/summer bloom (Figures 16 and 17). Model annual mean data are shown, but seasonal minima are not much less, compared to the strong summer drawdown in the observations.

Figure S10a – Global distribution of dissolved iron (dFe) measurements in the GEOTRACES (black/green) and PICES/MBARI (blue) data compilations. GEOTRACES Pacific data north of 25ºS are indicated in green. Blue dots outside the Pacific are MBARI data. Large symbols indicate stations along GA-02 that are compared in Figure S10h.

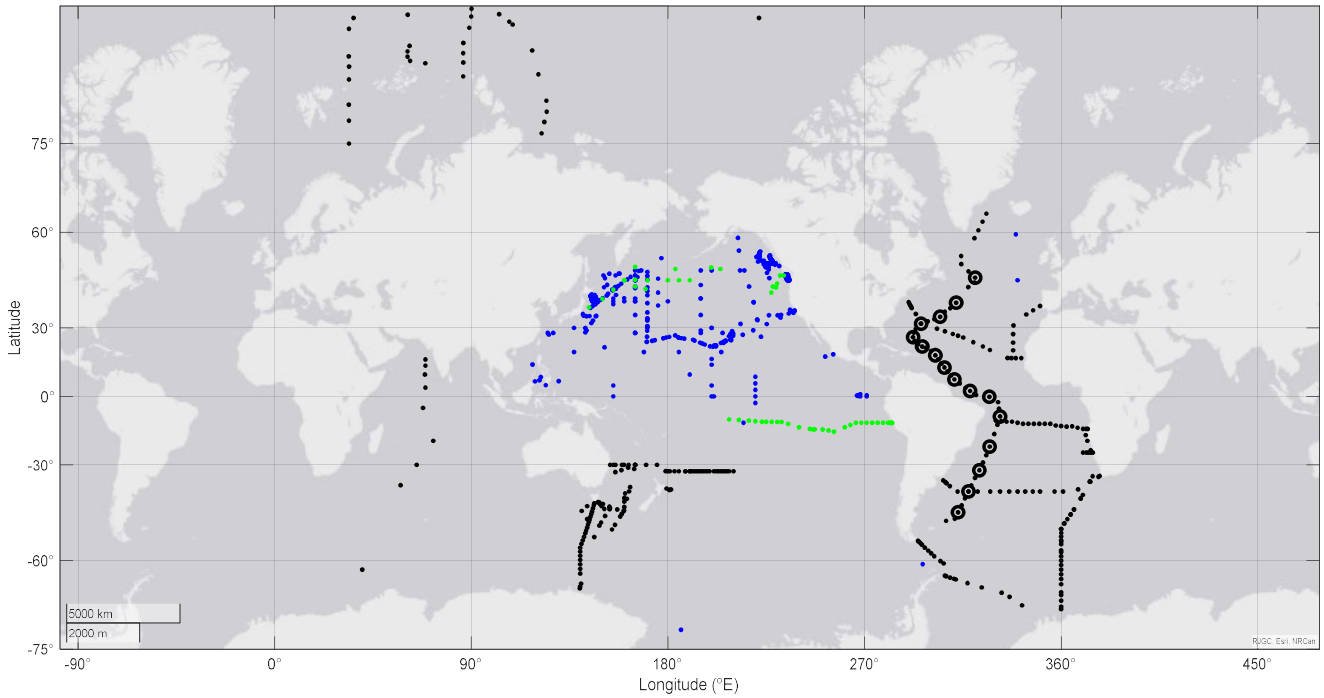

Figure S10b - All observations of dissolved iron (dFe) concentration (<2 nM) plotted against sampling depth. GEOTRACES data are in black and PICES/MBARI data are blue. Model data are global mean profiles of annual mean data as in Figure 13 in the main text.

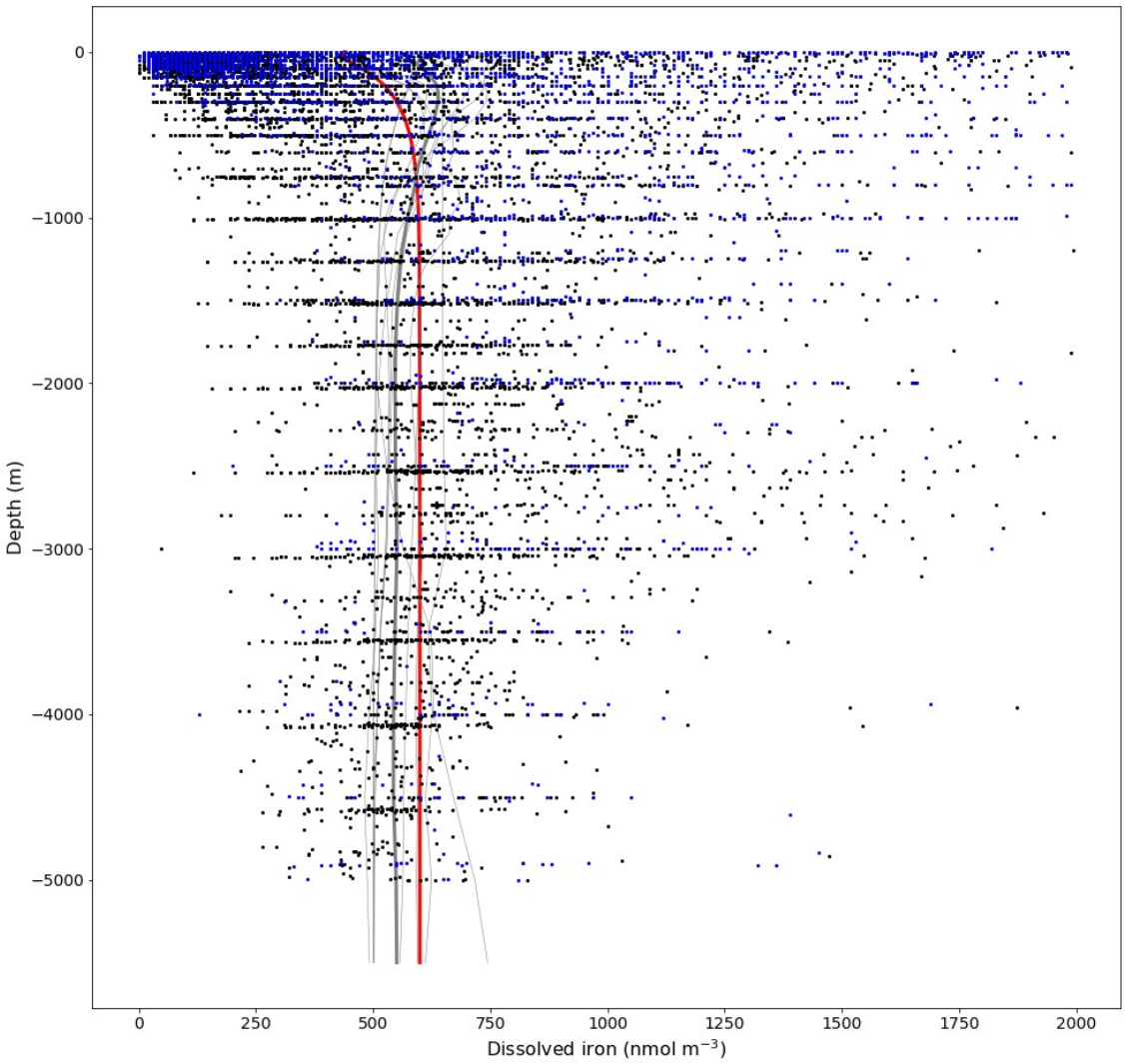

Figure S10c - Mean of observations of dissolved iron (dFe) concentration (<2 nM) for various depth strata, including both GEOTRACES and PICES/MBARI data. Means of all data available in that depth range; spatial coverage is very incomplete and inconsistent among the depth strata. Averaging layers are 50 m (0-1000 m), 100 m (1000-3000 m) or 300 m (>3000 m) thick. Model data are global mean profiles of annual mean data as in Figure 13 in the main text.

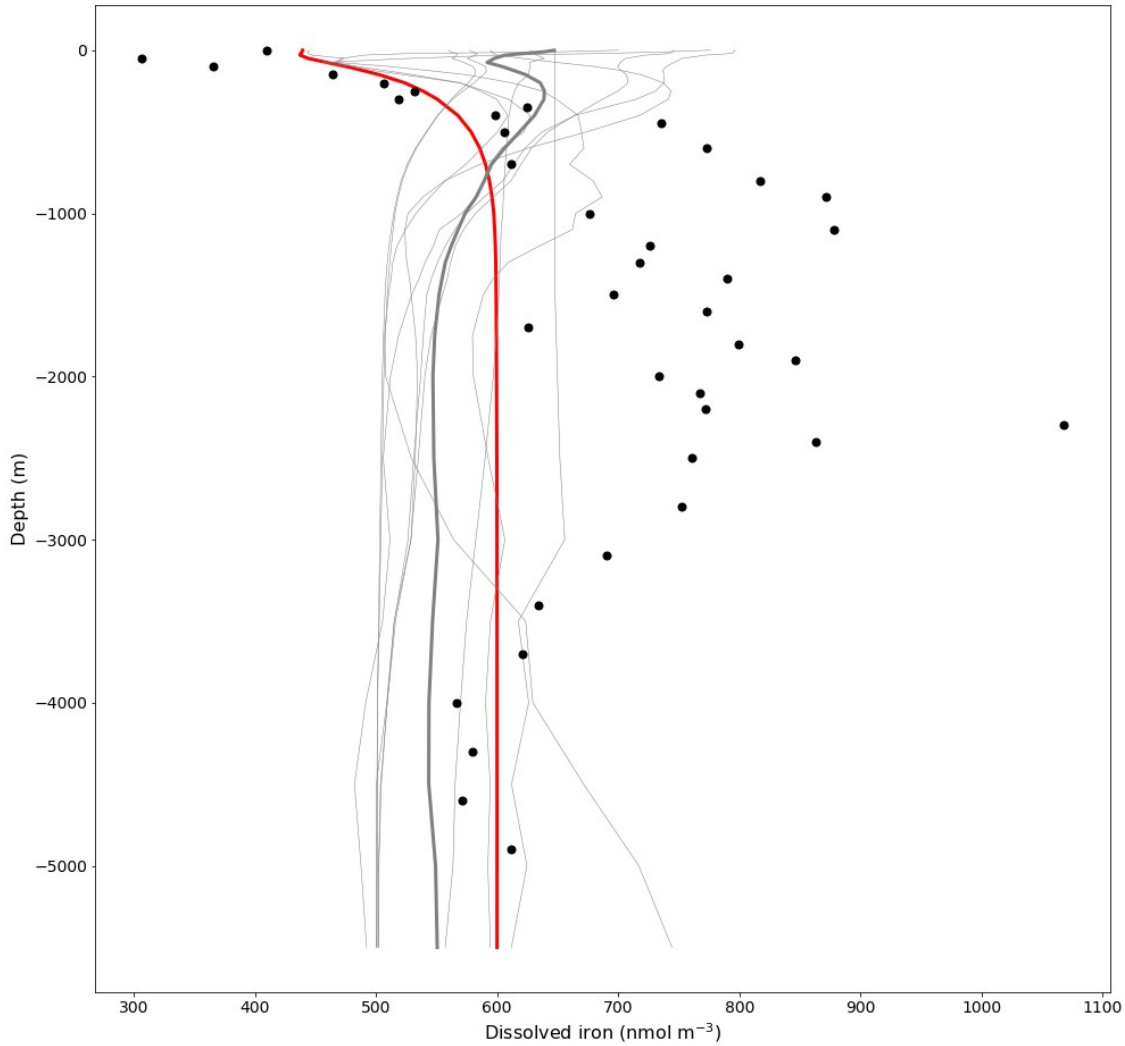

Figure S10d - Modelled and observed mean dissolved iron (dFe) concentrations (excluding those >2.5 nM) in the upper 50 m at locations where a depth profile was taken (N=1122). Observed data are means of all measurements made at depths <50 m within a given profile. Model data are climatological surface values for the month in which the observed data were collected (red: CanESM5-CanOE; black CNRM-ESM2-1; blue: GFDL-CM4; magenta: MPI-ESM1-2-LR). Selection of models is somewhat arbitrary but includes the models that show the highest overall skill according to the metrics shown in Figures S10e-g. Thin lines are linear regressions for individual models; thick black line is 1:1.

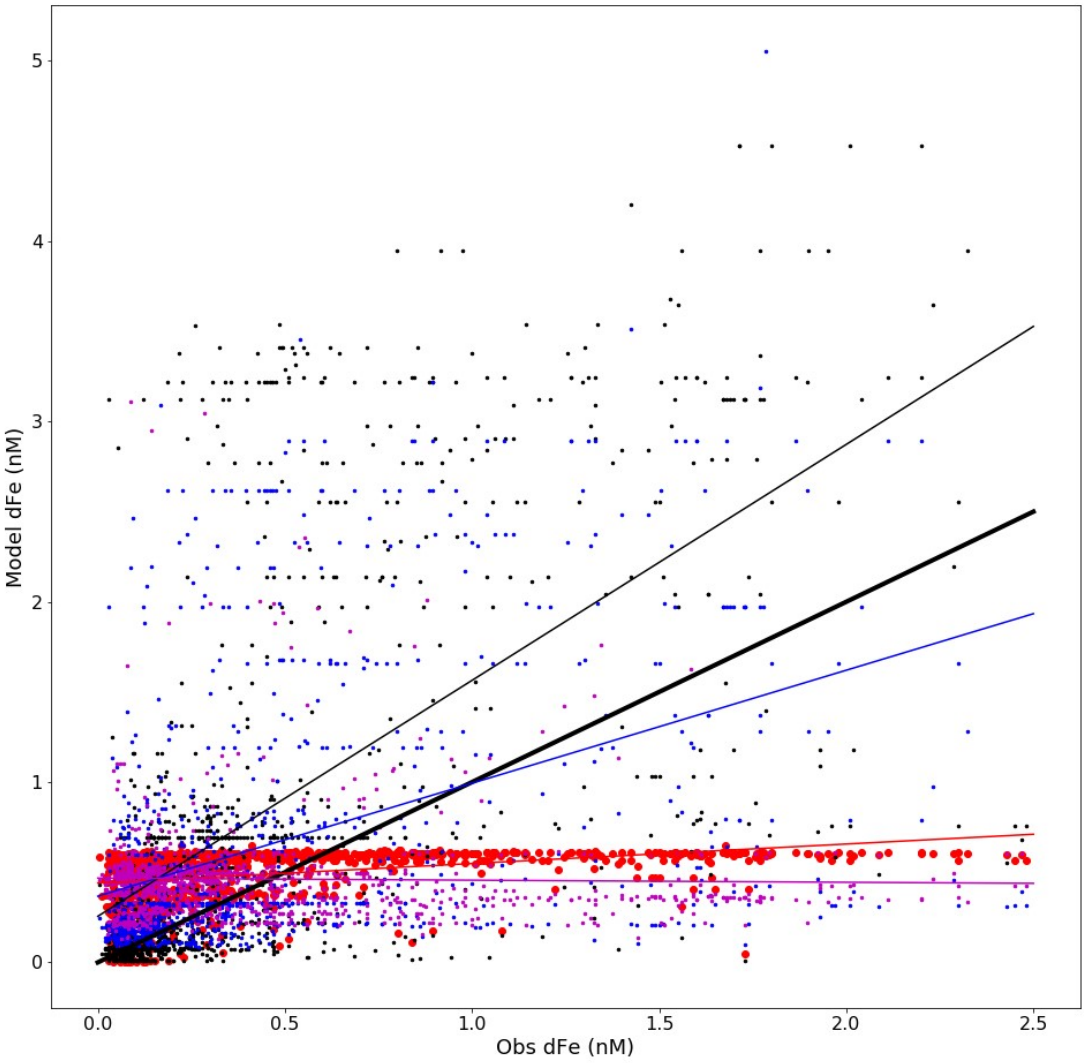

Figure S10e - Root mean square error and correlation coefficient for surface dissolved iron data (upper 50 m mean with maximum of 2.5 nM, as in Figure S10d) for CMIP6 models for which seasonal data were available.

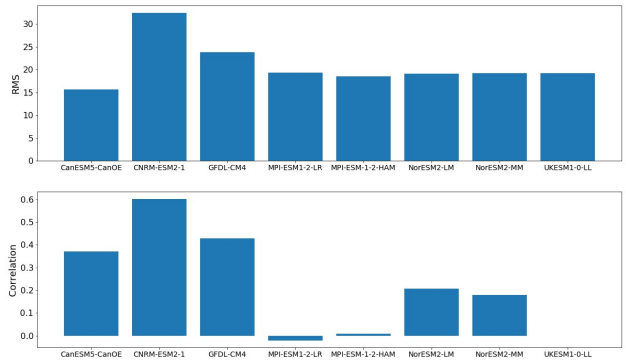

Figure S10f - As S10e but for the Pacific only (north of 25ºS).

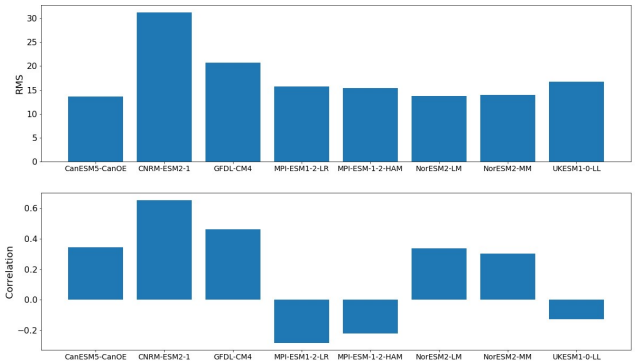

Figure S10g - As S10e but excluding the Pacific north of 25ºS.

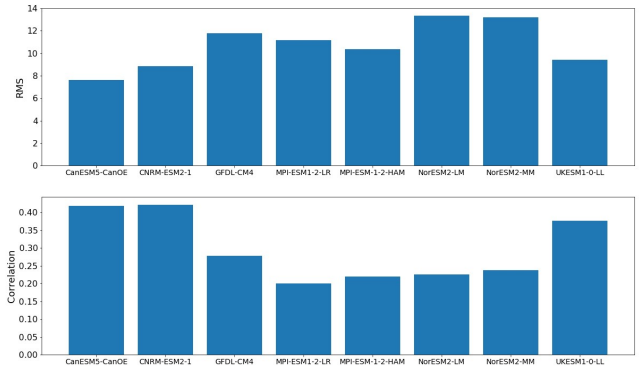

Figure S10h - Depth profiles for modelled and observed dissolved iron along the GA-02 transect of the Atlantic Ocean. Station locations are shown in Figure S10a (every third station, sorted by latitude). Model data are annual means.

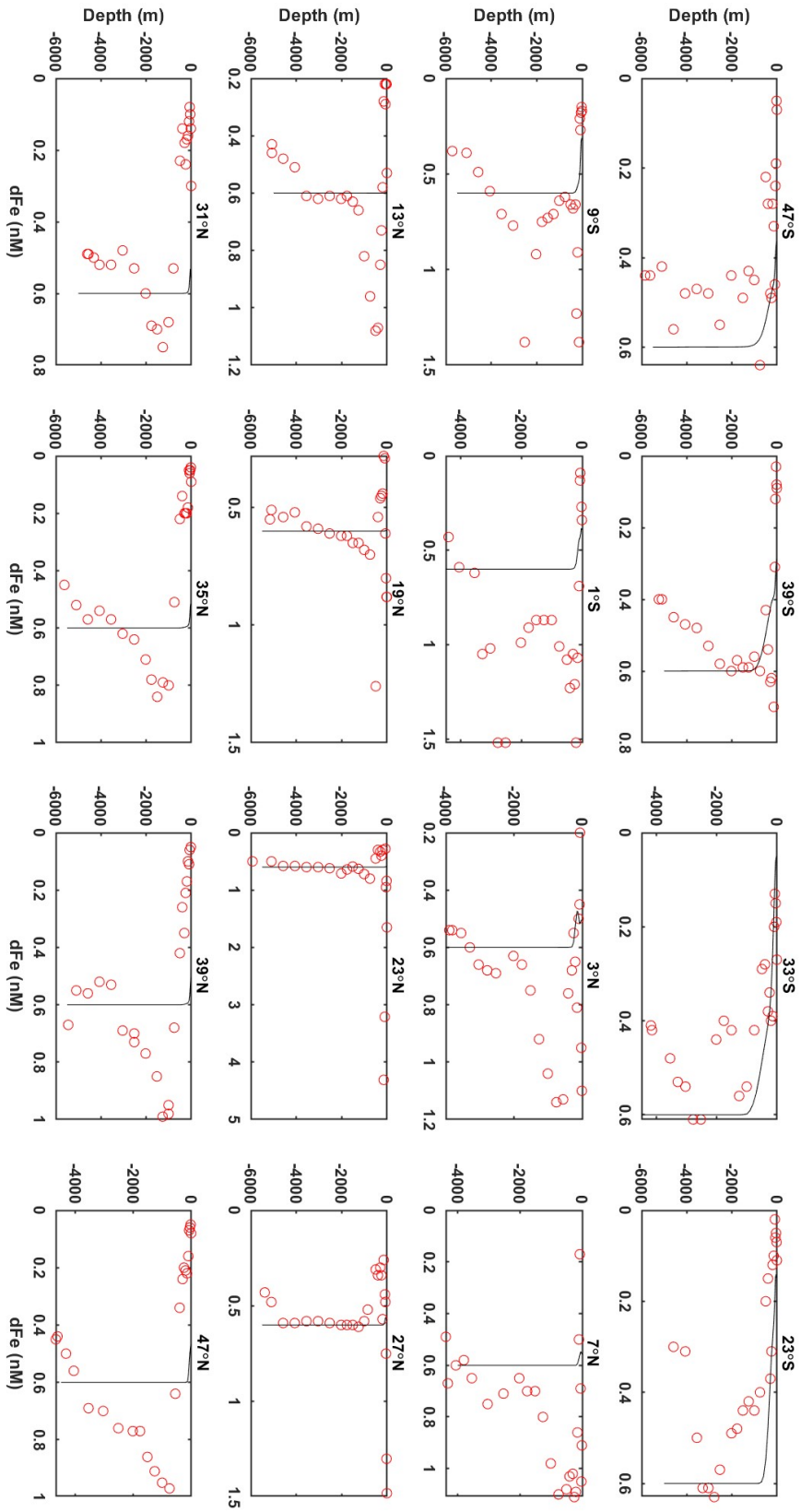

References

Middag, R., M.M.P. van Hulten, H.M. Van Aken, M.J.A. Rijkenberg, L.J.A. Gerringa, P. Laan, and H.J.W. de Baar, 2015. Dissolved aluminium in the ocean conveyor of theWest Atlantic Ocean: Effects of the biological cycle, scavenging, sediment resuspension and hydrography. Marine Chemistry 177: 69–86.

Resing, J.A., P.N. Sedwick, C.R. German, W.J. Jenkins, J.W. Moffett, B.M. Sohst and A. Tagliabue, 2015. Basin-scale transport of hydrothermal dissolved metals across the South Pacific Ocean. Nature 523: 200–203.

Séférian, R., et al., 2020. Tracking improvement in simulated marine biogeochemistry between CMIP5 and CMIP6, Current Climate Change Reports, 6: 95-119.

Schlitzer, R., et al., 2018. The GEOTRACES Intermediate Data Product 2017. Chemical Geology 493: 210-223.

The data file for the PICES WG22 data compilation requests that data users cite the original publications. As all of the data are used except for the SOLAS underway data, all of the original references are listed here:

Boyle, E.A., B.A. Bergquist, R.A. Kayser and N. Mahowald, 2005. Iron, manganese and lead at Hawaii Ocean Time-Series station ALOHA: Temporal variability and an intermediate water hydrothermal plume. Geochimca et Cosmochimica Acta, 69: 933-952.
Brown, M. T., W. M. Landing, and C. I. Measures, 2005. Dissolved and particulate Fe in the western and central North Pacific: Results from the 2002 IOC cruise. Geochem, Geophys. Geosyst., 6, Q10001, doi: 10.1029/2004GC000893.
Bruland, K., Orians, K. and Cowen, P. ,1994. Reactive trace metals in the stratified central North Pacific. Geochem. Cosmochim. Acta. 58, 3171-3182.
Coale, K. H., Fitzwater, S. E., Gordon, R. M., Johnson, K. S. and Barber, R. T., 1996a. Control of community growth and export production by upwelled iron the equatorial Pacific Ocean. Nature, 379:621-624.
Ezoe M , Ishita T , Kinugasa M , Lai X, Norisuye K, Sohrin Y, 2004, Distributions of dissolved and acid-dissolvable bioactive trace metals in the North Pacific Ocean. Geochemical Journal, 38(6), 535-550.
Fitzwater, S.E., K.H. Coale, R.M. Gordon, K.S. Johnson, M.E. Ondrusek, 1996, Iron deficiency and phytoplankton growth in the equatorial Pacific, Deep-Sea Res. II, 43, 995-1015
Fujishima, Y., K. Ueda, M. Maruo, E. Nakayama, C.Tokutome, H.Hasegawa M. Matsui and Y. Sohrin. Distribution of Trace Bioelements in the Subarctic North Pacific Ocean and the Bering Sea (the R/V Hakuhou Maru Cruise KH-97-2), Journal of Oceanography, Vol. 57, pp.261 to 273, 2001
Gordon, R. M., Johnson, K. S. and Coale, K. H., 1998. The behavior of iron and other trace elements during the IronEx I and PlumEx experiments in the equatorial Pacific. Deep-Sea Res. II 45: 995-1041.
Gordon, R.M. , J.H. Martin, G.A. Knauer, 1982, Iron in north-east Pacific waters, Nature, 299, 611-612
Johnson - MLML World Iron Data Set: Appendix A to Johnson, K. S., Gordon, R. M. and Coale, K. H., 1997, What controls dissolved iron concentrations in the world ocean? Mar. Chem. 57: 137-161.
Johnson, K.S., Elrod, V., Fitzwater, S., Plant, J.N., Chavez, F.P., Tanner, S.J., Gordon, M., Westphal, D.L., Perry, K.D., Wu, J., and Karl, D.M., 2003. Surface ocean-lower atmosphere interactions in the

Northeast Pacific Ocean Gyre: Aerosols, iron, and the ecosystem response, GBC(17), 10.1029/2002GB002004
Johnson, K.S., F.P. Chavez, V.A. Elrod, S.E. Fitzwater, J.T. Pennington, K.R. Buck, and P.M. Walz, 2001. The annual cycle of iron and the biological response in central California coastal waters. Geophys. Res. Letters 28: 1247-1250.
Johnson, WK, Miller, LA, Sutherland, ND, Wong, CS, 2005. Iron transport by mesoscale Haida eddies in the Gulf of Alaska, Deep-Sea Res. II, 52: 933-953.
Kitayama, S., K. Kuma, E. Manabe, K. Sugie, H. Takata, Y. Isoda,K.Toda,S.Saitoh,S.Takagi,Y.Kamei,and K.Sakaoka,2009.Controls on iron distributions in the deep water column of the North Paciffic Ocean:iron(?) hydroxide solubility and humictype fluorescent dissolved organic matter.J.Geophys.Res.,114:C08019,doi:10.1029/2008JC004754
Kondo, Y., 2007. Dynamics of the organic Fe complexing ligands and phytoplankton in the Pacific Ocean.The University of Tokyo. Ph.D.Thesis, 256pp.
Kondo, Y., S. Takeda and K. Furuya, 2012. Distinct trends in dissolved Fe speciation between shallow and deep waters in the Pacific Ocean. Marine Chemistry, 134–135, 18–28
Kuma, K, J. Nishioka, K. Matsunaga, 1996, Controls on iron (III) hydroxide solubility in seawater: The influence of pH and natural organic chelators, Limnol. Oceanogr., 41, 396-407
Kuma, K., A. Katsumoto, H. Kawakami, F. Takatori, K. Matsunaga,1998, Spatial variability of Fe(III) hydroxide solubility in the water column of the northern North Pacific Ocean, Deep-Sea Res. I, 45, 91-113
Kuma, K., Isoda, Y. and Nakabayashi, S., 2003, Control on dissolved iron concentrations in deep waters in the western North Pacific: Iron(III) hydroxide solubility. J. Geophys. Res., 108 (C9): 3289, doi:10.1029/2002JC001481 (2003).
Landing, W.M., K.W. Bruland, 1987, The contrasting biogeochemistry of iron and manganese in the Pacific Ocean, Geochim. et Cosmo. Acta, 51, 29-43
Mackey, D.J., J.E. O'Sullivan, R.J. Watson, 2002, Iron in the western Pacific: A riverine or hydrothermal source for iron in the Equatorial Undercurrnet?, Deep-Sea Res. I, 49, 877-893
Martin, J.H. and R.M. Gordon, 1988, Northeast Pacific iron distributions in relation to phytoplankton productivity, Deep-Sea Res. I, 35, 177-196
Martin, J.H., R.M. Gordon, S. Fitzwater, W.W. Broenkow, 1989, VERTEX: phytoplankton/iron studies in the Gulf of Alaska, Deep-Sea Res., 36, 649-680
Nakabayashi, S., K. Kuma, K. Sasaoka, S. Saitoh, M. Mochizuki,, N. Shiga, and M. Kusakabe, 2002. Variation in iron(III) solubility and iron concentration in the northwestern North Pacific Ocean. Limnol. Oceanogr. 47: 885-892
Nakabayashi, S., M. Kusakabe, K. Kuma, and I. Kudo, 2001. Vertical distributions of Iron(III) hydroxide solubility and dissolved iron in the northwestern North Pacific Ocean. Geophys. Res. Letters 28: 4611-4614.
Nishioka, J., S. Takeda, I. Kudo, D. Tsumune, T. Yoshimura, K. Kuma, A. Tsuda, 2003, Size-fractionated iron distributions and iron-limitation processes in the subarctic NW Pacific, GRL, 30, NO. 14, 1730, doi:10.1029/2002GL016853.
Nishioka, J., T. Ono, H. Saito, K. Sakaoka, and T. Yoshimura (2011),Oceanic iron supply mechanisms which support the spring diatom bloom in the Oyasio region,western subarctic Pacific,J.Geophys.Res.,116,C02021,doi:10.1029/2010JC006321
Nishioka, J., T. Ono, H. Saito, T. Nakatsuka, S. Takeda, T. Yoshimura, K. Suzuki, K. Kuma, S. Nakabayashi, D. Tsumune, H. Mitsudera, W. K. Johnson, A. Tsuda, (2007) Iron input into the western subarctic Pacific, importance of iron export from the Sea of Okhotsk, Journal of Geophysical Research, 112, C10012, doi:10.1029/2006JC004055.
Nishioka, J., Takeda, S., Wong, C., Johnson, W. 2001. Size-fractionated iron concentrations in the northeast Pacific Ocean: Distribution of soluble and small colloidal iron. Mar. Chem. 74, 157-179

Obata H., 1997. Development of an automated analytical method of iron in seawater and studies on the behavior of iron in the ocean.Kyoto University.Ph.D.Thesis,109pp.
Obata, H., H. Karatani and E. Nakayama, 1993. Automated determination of iron in seawater by chelating resin concentration and chemiluminescence detection.Analytical Chemistry,65:1524-1528
Obata, H., H. Karatani, M. Matsui and E. Nakayama, 1997. Fundamental studies for chemical speciation of iron in seawater with an improved analytical method.Marine Chemistry,56:97-106
Roy, E., 2009. The detection and biogeochemistry of trace metals in natural waters. Ph.D. Thesis, University of Maine.
Rue, E.L. and K.W. Bruland, 1995. Complexation of iron(III) by natural organic ligands in the central North Pacific as determined by a new competitive ligand equilibration/adsorptive cathodic stripping voltammetric method. Mar. Chem. 50: 117-138.
Takata, H, Kuma, K, Saitoh, Y, Chikira, M, Saitoh, S, Isoda, Y, Takagi, S, Sakaoka, K, 2006. Comparing the vertical distribution of iron in the eastern and western North Pacific Ocean. Geophys. Res. Lett., 33, L02613, doi:10.1029/2005GL024538, 2006.
Takata, H., K. Kuma, S. Iwade, Y. Yamajyoh, A. Yamaguchi, S. Takagi, K. Sakaoka, Y. Yamashita, E. Tanoue, T. Midorikawa, K. Kimura, J. Nishioka, 2004, Spatial variability of iron in the surface water of the northwestern North Pacific Ocean, Mar. Chem., 86, 139-157
Takeda, S., H. Obata, 1995, Response of equatorial Pacific phytoplankton to subnanomolar Fe enrichment, Mar. Chem, 50, 219-227
Tsuda, A., S. Takeda, H. Saito, J. Nishioka, Y. Nojiri, I. Kudo and others, 2003, A mesoscale iron enrichment in the western Subarctic Pacific induces a large centric diatom bloom, Science, 300, 958-961
Wu, J., E. Boyle, W. Sunda, and L.-S. Wen, 2001. Soluble and colloidal iron in the oligotrophic North Atlantic and North Pacific. Science 293: 847-849.